Pharmacogn. Res., 2024; 16(2):244-253.
https://www.phcogres.com

Original Article

In silico and Biological Screening of Phytochemicals against NMDA Receptor for Alzheimer's Disease Therapeutics

Bhushan Arun Baviskar, Sharada Laxman Deore, Bhavana Ashok Shende*, Somshekhar Khadabadi, Anjali Ashokrao Kide

Government College of Pharmacy, Kathora Naka, Amravati, Maharashtra, INDIA.

ABSTRACT

Background: Alzheimer's Disease (AD), characterized by irreversible neurodegeneration and cognitive decline, lacks a definitive cure, and current medications merely alleviate symptoms. Cognitive manifestations in AD are linked to disrupted glutamatergic neurotransmission, where β-Amyloid (A) accumulation at specific synapses interacts with glutamine synthetase, causing enzyme inactivation and subsequent NMDA signalling impairment. Dysregulation of glutamine synthetase leads to NMDA receptor hyper activation, resulting in neuronal damage and cell death. **Aim:** The focus of this investigation is on N-Methyl D-Aspartate (NMDA) receptors, which belong to the ionotropic glutamate receptor family and play vital roles in various physiological and pathological processes such as neuron development, synaptic plasticity, and central nervous system learning and memory. This study seeks to analyze target data to differentiate between effective and ineffective options for virtual screening. Utilizing this information, the study aims to generate a novel or enhanced reaction product. **Materials and Methods:** Computational embedding was employed to explore interactions between NMDA receptors and phytoconstituents of selected plants, including Amla, Shankhapushpi, Giloy, Ashwagandha, and Turmeric. ADMET descriptions for well-known botanical compounds were also scrutinized. **Results:** Structural analysis of 75 compounds derived from selected phytochemicals was conducted based on molecular properties. Key compounds were identified, and additional ADMET properties were evaluated. Quercetin emerged as the top-ranking compound based on shear score, shear strength, and molecular interactions with NMDA receptors. **Conclusion:** This computational study identifies specific plants as potential NMDA receptor antagonists, offering promise for mitigating Alzheimer's disease symptoms in the future.

Keywords: Alzheimer's disease, Molecular docking, N-methyl-D-aspartate-receptor, ADMET descriptions, Dock ligands, Computational embedding, Quercetin.

Correspondence:
Ms. Bhavana Shende
Research Scholar, Government College of Pharmacy, Kathora Naka, Amravati-444604, Maharashtra, INDIA.
Email: bhavana11121994@gmail.com

Received: 29-09-2023;
Revised: 17-12-2023;
Accepted: 16-02-2024.

INTRODUCTION

N-Methyl-d-Aspartate Receptors (NMDARs) function as glutamate-gated ion channels, playing a crucial role in both normal brain physiology and pathological conditions. Due to the association of many pathological states with NMDAR hyper activation, there is potential therapeutic value in subunit-selective antagonists, particularly those targeting GluN2B receptors, which have shown the most efficacy among NMDAR-targeted drugs.[1] The discovery of Ifenprodil marked a significant milestone, leading to the identification of various GluN2B-selective compounds with unique structural motifs. Despite the molecular distinctions observed, little empirical data support the existence of different binding regions. Through X-ray crystallography, it was found that EVT-101, a structurally distinct GluN2B antagonist from the classical phenyl ethanolamine pharmacophore, binds to the same GluN1/GluN2B dimer interface as Ifenprodil. Importantly, EVT-101 exhibits distinct binding modes that influence receptor interactions, as confirmed by mutagenesis experiments.[2] Computational analysis further categorizes GluN2B-selective antagonists into two distinct classes based on their interactions, expanding the allosteric and pharmacological understanding of NMDARs and offering a new structural model for the development of next-generation GluN2B antagonists with therapeutic potential in the brain.[3] Research indicates that cognitive symptoms in Alzheimer's Disease (AD) arise from compromised brain function, particularly in glutamatergic neurotransmission. This dysfunction involves the accumulation of β-Amyloid (A) at specific synapses, leading to interactions with glutamine synthetase and subsequent enzyme inactivation, resulting in the release of the NMDA signalling pathway.[4] Treatments targeting glutamatergic neurotransmission within the glutamatergic system have shown promise in preventing

DOI: 10.5530/pres.16.2.31

subsequent neuronal damage and death.[5] Memantine, a synthetic compound and non-competitive voltage-dependent NMDA receptor antagonist, is currently the sole FDA-approved drug for moderate to severe Alzheimer's disease. Despite its clinical efficacy, Memantine is associated with various side effects, including hallucinations, dizziness, headache, vomiting, and urinary tract infections.[6,7] Recognizing the neuroprotective properties of Memantine demonstrated in prior studies, extensive research is underway to identify new NMDA receptor ligands with reduced or no side effects. This study aims to develop an *in silico* method to identify potential NMDA receptor antagonists from selected Ayurvedic plants, such as Indian gooseberry, Shankhapushpi, Giloy, Ashwagandha, and turmeric. The goal is to utilize model-based virtual analysis to assess the binding mechanisms, interactions, and molecular effects of plant phytochemicals that inhibiting the NMDA receptor-mediated response.[8]

MATERIALS AND METHODS

Synthesis of Receptor Protein

The X-ray crystal structure of the NMDA receptor was acquired from the Protein Data Bank (PDB) maintained by the Structural Bioinformatics Research Collaborative Laboratory. The PDB houses various crystal structures of the NR1 binding core, specifically the glycine B site. In this study, we utilized a 1.90 resolution crystal structure of the NR1 ligand-binding core associated with the antagonist 5, 7-dichloroquinuric acid (DCKA) obtained from the PDB.[9] DCKA was chosen for its ability to identify the active site, given its substantial size, resulting in the largest binding pocket available.[10] For instance, the glycine-bound GluN1, 1PB7 exhibited a binding pocket of 93.26 Å, whereas 1PBQ displayed a binding pocket of 198.56 Å.[11] Furthermore, 1PBQ serves as a unique example showcasing a disorder in the ligand-binding domain of the NMDA receptor subunit.[12] To prepare the acceptor protein, the protein preparation wizard workflow within the Schrödinger suite was employed. This involved the addition of hydrogen atoms, establishment of bonds, and the removal of all water molecules except those associated with the active site. For ligand preparation, the LigPrep panel in the software was employed. LigPrep facilitated the creation of a low-energy 3D model with the correct chirality for each step in the input sequence. All models in MAE format were imported into the project file, and the OPLS 2005 force field was applied for ligand preparation.[13] Potential ionization states for all samples at pH 7.0±2.0 were determined using a selective ionizer. Only one low-energy ring conformer per ligand was allowed. Each ligand formed 32 low-energy stereoisomers to account for other chiral atoms in the structure and generate additional structures with the same molecular composition but varied chiral arrangements.[14]

Selection of the Receptor

Docking studies were carried out using NMDA glutamate receptor structure (TRANSPORT PROTEIN) complexed with an inhibitor, QEL 503 (IFENPRODIL). It was solved by X-ray diffraction techniques with a resolution of 2.77 Å. We retrieved it from the Brookhaven protein database (code 5EWJ).

Details

Source: Organism Scientific: *Homo sapiens*;

Source: Organism Common: Human;

Source: Expression System: Spodoptera Frugiperda;

Source: Expression System Taxid: 7108;

Source: Expression System Vector Type: Baculovirus.

N-Methyl-d-Aspartate Receptors (NMDARs) are glutamate-gated ion channels that play key roles in brain physiology and pathology. Because numerous pathologic conditions involve NMDAR over activation, subunit-selective antagonists hold strong therapeutic potential, although clinical successes remain limited. Among the most promising NMDAR-targeting drugs are allosteric inhibitors of GluN2B-containing receptors. Since the discovery of Ifenprodil, a range of GluN2B-selective compounds with strikingly different structural motifs have been identified. This molecular diversity raises the possibility of distinct binding sites, although supporting data are lacking. Using X-ray crystallography, authors shown that EVT-101, a GluN2B antagonist structurally unrelated to the classic phenyl ethanolamine pharmacophore, binds at the same GluN1/GluN2B dimer interface as Ifenprodil but adopts a remarkably different binding mode involving a distinct sub cavity and receptor interactions. Mutagenesis experiments demonstrate that this novel binding site is physiologically relevant. Moreover, *in silico* docking unveils that GluN2B-selective antagonists broadly divide into two distinct classes according to binding pose. These data widen the allosteric and pharmacological landscape of NMDARs and offer a renewed structural framework for designing next-generation GluN2B antagonists with therapeutic value for brain disorders.

Ligand Preparation

The ligand preparation process involved the application of the Lig Prep panel within the software. The use of Lig Prep resulted in the generation of a single low energy 3D structure with the accurate chiralities for each input structure that successfully underwent processing. All structures in MAE format were imported in to the project file and subjected to ligand preparation, employing the OPLS 2005 force field. Potential ionization states for each structure at pH 7.0±2.0 were symmetrically determined using the ionizer option, allowing the generation of only one low energy ring conformer per ligand. Furthermore, the generation of 32 low energy stereoisomers per ligands was permitted, aiming to

identify additional chiral atoms in the structures and generate supplementary structures with the same molecular formula but distinct chiral properties.

Preparation of Protein Protein Ligand Complex

The reliability of outcomes derived from Glide is significantly contingent on the quality of the initial structures.[15] These starting structures are required to encompass all hydrogen atoms, possess accurate charge states in the vicinity of the binding site, and exhibit lack of substantial steric clashes. A typical protein complex structure obtained from the Research Collaboratory for Structural Bioinformatics (RCSB) website (http://www.rcsb.org) in PDB format lacks hydrogen atoms and may feature residues in nonstandard charge states.[16] Consequently, thorough protein preparation process was undertaken to ensure chemical accuracy and optimize the protein structure for achieving optimal results.[17]

The 5EWJ.pdb file was imported in to Maestro. The human beta-secretase enzyme structure is composed of two chains, along with some water molecules ad the ligand QEL 503. All other ligands and water molecules, except for QEL 503, were removed.[18]

In the protein preparation and refinement process, the Neutralization zone around the ligand was set to 'On' with an RMSD of 0.30 Å of the ligand was neutralized.[19] A series of restrained partial minimizations of the cocrystallized complex were conducted to optimize the positions of newly added hydrogen and alleviate any strain arising from unphysical short distances in the X-ray structure, as part of the refinement process.[20] The resulting optimized receptor structure is depicted in Figure 1, while the structure of the cocrystallized ligand QEL 503 is presented in Figure 2.

Receptor Grid Generation

Grid files embody the physical characteristics of a receptor volume, particularly the active site, which will be explored in ligand docking endeavors. The calculated grid file is employed in the subsequent step for ligand docking. The enclosing purple box delinerates the protein volume for which grids will be calculated, as illustrated in Figure 3. The chosen center option is the Centroid of the workspace ligand. No constraints were applied during the grid preparation process.

Docking of Ligands

Ligand docking was performed in XP (Extra Precision) mode. The flexible docking included allowable flips of 5- and 6-member rings. Sets of ligands were docked and scored without incorporating or relying on similarity scores. Supplementary filters were applied, and configurations were adjusted to collect and record one pose for each ligand in the pose viewer file. The Van der Waals radius scaling for ligand atoms was set to default values: scaling by 0.80 for atoms with a partial atomic charge less than 0.15.

Validation of Docking Process

The screening accuracy was assessed by repetition of docking process with the same parameters for above series of compounds seeded with series of known inhibitors. The structures of compounds used for validation are shown in Figure 4.

Computing Platforms

Docking computations were executed on Intel (R) Core (TM) i5-1035G1 CPU with a 1.19 GHz processor, Operating System-Windows 10 and 8 GB RAM with NVIDIA Graphics

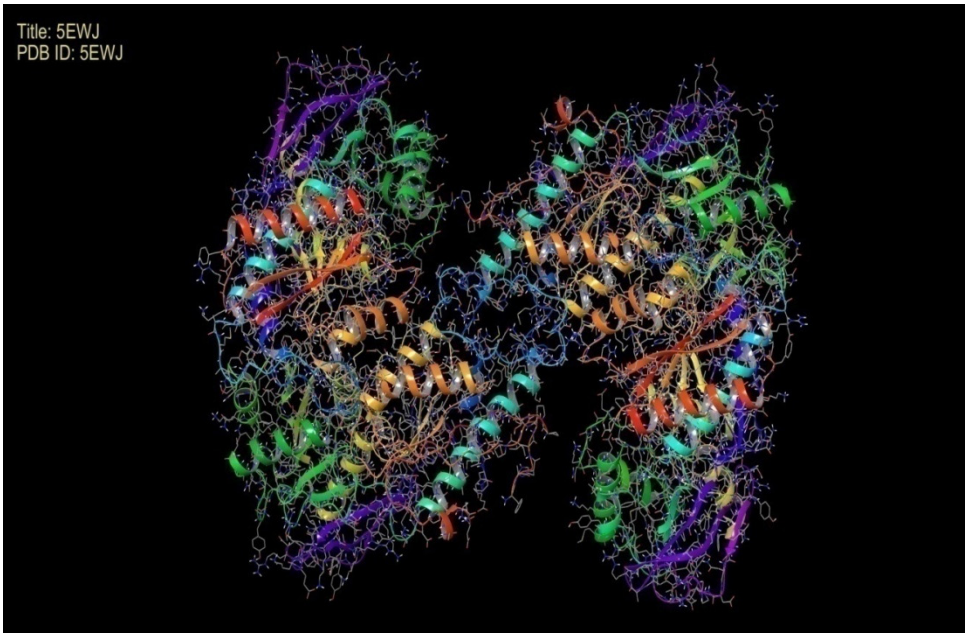

Figure 1: 5EWJ receptor structure.

Card. Average time required for docking was 1.2 min/molecule in the XP mode.

RESULTS

Ligand Preparation and Docking

Ligand poses generated by Glide undergo a sequential application of hierarchical filters for examination of ligand-receptor interactions. These filters initially evaluate the ligand's compatibility with the identified functional region, employing a grid based approach, aiming to reduce the unbound ligand-receptor interaction energy according to OPLS-AA subsequently; weaker poses receive a final score. Taxi profit analysis prioritizes visual metrics over numerical metrics, with Glide displayed through the Glide Exposure Viewer panel. The Table 1 provides information on the Glide score (G-Score), G-Energy, and insertion scores for each pose and the corresponding pose receptor combination. Table 1 presents the outcomes for each compound and molecular group utilized in the validation process. For the analysis of insertion results, compounds were chosen based on the best conformation score predicted by the function score as indicated in Table 1. All potential ligands were drawn using build panel in maestro graphical user interface and saved in .mol format (MDL MOL Format). The numbers of ligands chosen for docking.

Docking Studies

The Glide (version 10.0, Schrödinger, LLC, New York, NY, 2005) software was used to dock potential inhibitors (Ligand) in the binding pocket of the beta-secretase enzyme structure. Glide is most commonly used and validated software designed to assist in

Table 1: Molecular interaction of top lead phytoconstituents with N-methyl-D-aspartate receptor.

Phytochemicals	Docking score	Glide score	Glide energy	H-Bond
QEL 503	-9.745	-9.745	-68.239	SER A:132 (01) GLN B: 110 (02) GLU B: 106 (01)
Anaferine	-7.326	-7.326	-37.747	TYR A: 109(01) GLN B:110(01)
Withhasomnine	-6.662	-6.662	-27.102	No hydrogen bond found
Withaferin A	-5.842	-5.842	-25.235	ASP B:113 (01) GLU B:236(01) ARG A:115(01)
Quercetin	-7.103	-7.103	-47.594	THR A: 333(01), ILE A: 133(01), SER A: 132(01), GLN B:110(01), GLU B:106(01)
Kaempferol	-6.905	-6.905	-46.156	ILE A: 133(01), SER A: 132(01), GLU B: 105(01)
Ellagic acid	-6.242	-6.242	-43.863	SER A: 132(01) ILE A: 133(01)
Cholorogenic acid	-9.679	-9.679	-64.531	ASP B: 136 (02) SER A: 132 (01) ILE A: 133 (01) GLN B:110 (01
Scopoletin	-6.36	-6.36	-33.539	GLU B:106(01)
Convolamine	-6.142	-6.142	-33.703	ARG A:115(01)
Hexahydrocurcumin	-8.956	-8.956	-49.677	LEU A:135(01) GLU B:106(01) ILE A:133(01)
Dihydrocurcumin	-8.314	-8.314	-60.746	SER A:132(01) ASP B:136(01)
Curcumin glucuronide sulfate	-8.258	-8.258	-66.755	SER A: 132(01) ASP B:138(01)

high-throughput screening of potential ligands based on binding mode and affinity for a given receptor molecule. One can compare ligand scores with those of other test ligands, or compare ligand geometries with those of a reference ligand. Glide approximates a complete systematic search of the conformational, orientational, and positional space of the docked ligand.

ADME/Pharmacokinetic Studies

All phytoconstituents were also analyzed for pharmacokinetic properties, in accordance with Lipinski's rule of five to know if the lead phytoconstituents can be administrated orally in the human body. The rule says that the compound should have hydrogen donor <5, hydrogen acceptor should be <10, molecular weight of <500 daltons, that none of the phytoconstituents violated the rule except Anaferine. Their octanol-water partition coefficient was above five though they were still following the Lipinski's rule of five as the drug which was to be formulated orally should have no more than one violation. When predicted for toxicological property all the top leads were found to be noncarcinogenic in rodent, mouse as well as rat model and nonmutagenic in Salmonella typhimurium model. Swiss ADME software is used (Table 3) for ADME/Pharmacokinetic Studies.

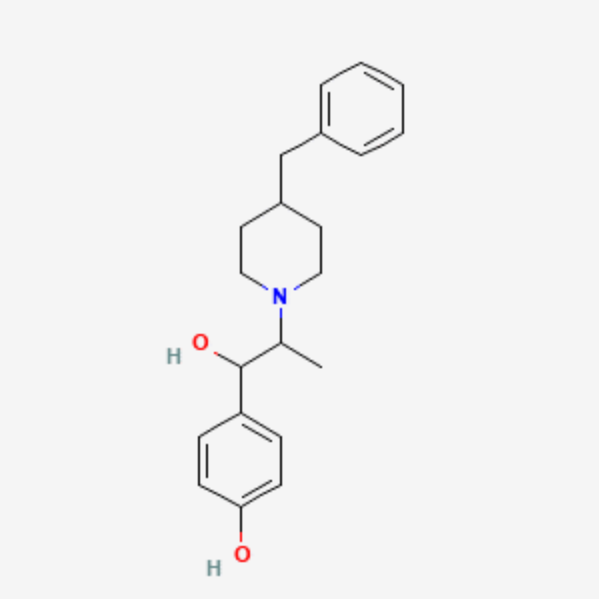

Figure 2: Cocrystalized ligand QEL 503 (IFENPRODIL).

Toxicity Studies

Withasomnine, quercetin, ellagic acid, chlorogenic acid, scopoletin, Dihydrocurcuminin, Curcumin glucoronide sulfate

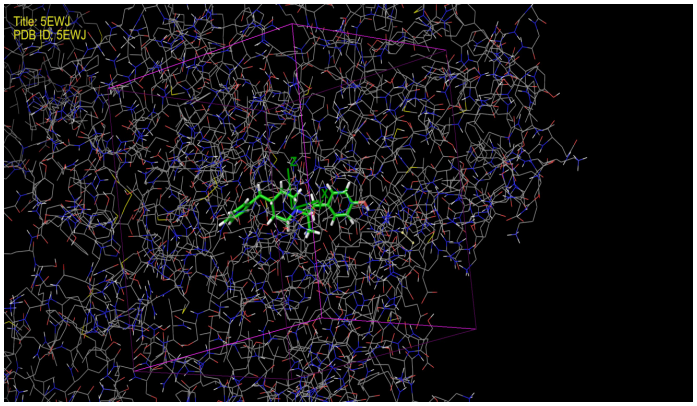

Figure 3: The marked ligand (QEL 503) with enclosing grid box (Pink Color).

Table 2: Top lead phytoconstituents with mol wt. and Lipinski's rule.

Phytoconstituents	Mol. Wt. g/mol	BBB partition coefficient	H-Bond Acceptors	H-Bond Donors	Log Po/w	GI Absorption	Lipinskis rule
Anaferin	224.34 g/mol	High	Yes	2.78	3	2	Yes; 0 violation
Withasomnine	184.24 g/mol	High	Yes	2.10	1	0	Yes; 0 violation
Withasomniferine A	470.60 g/mol	High	No	3.74	6	2	Yes; 0 violation
Quercetin	302.24 g/mol	No	7	5	1.63	High	Yes; 0 violation
Kaempferol	288.25 g/mol	No	6	4	1.42	High	Yes; 0 violation
Ellagic acid	302.19 g/mol	No	8	4	0.79	High	Yes; 0 violation
Chlorogenic acid	352.34 g/mol	Low	No	0.06	8	6	Yes; 1 violation: NHorOH>5
Scopoletin	192.17 g/mol	High	Yes	1.86	4	1	Yes; 0 violation
Convolamine	305.37 g/mol	High	Yes	3.41	5	0	Yes; 0 violation
Hexahydrocurcumine	530.61 g/mol	Low	No	4.29	3	9	Yes; 1 violation: MW>500
Dihydrocurcumine	370.40 g/mol	High	No	3.58	3	6	Yes; 0 violation
CurcumineGlucoronide sulphate	604.62 g/mol	Low	No	0.00	12	No; 2 violations: MW>500, NorO>10	12

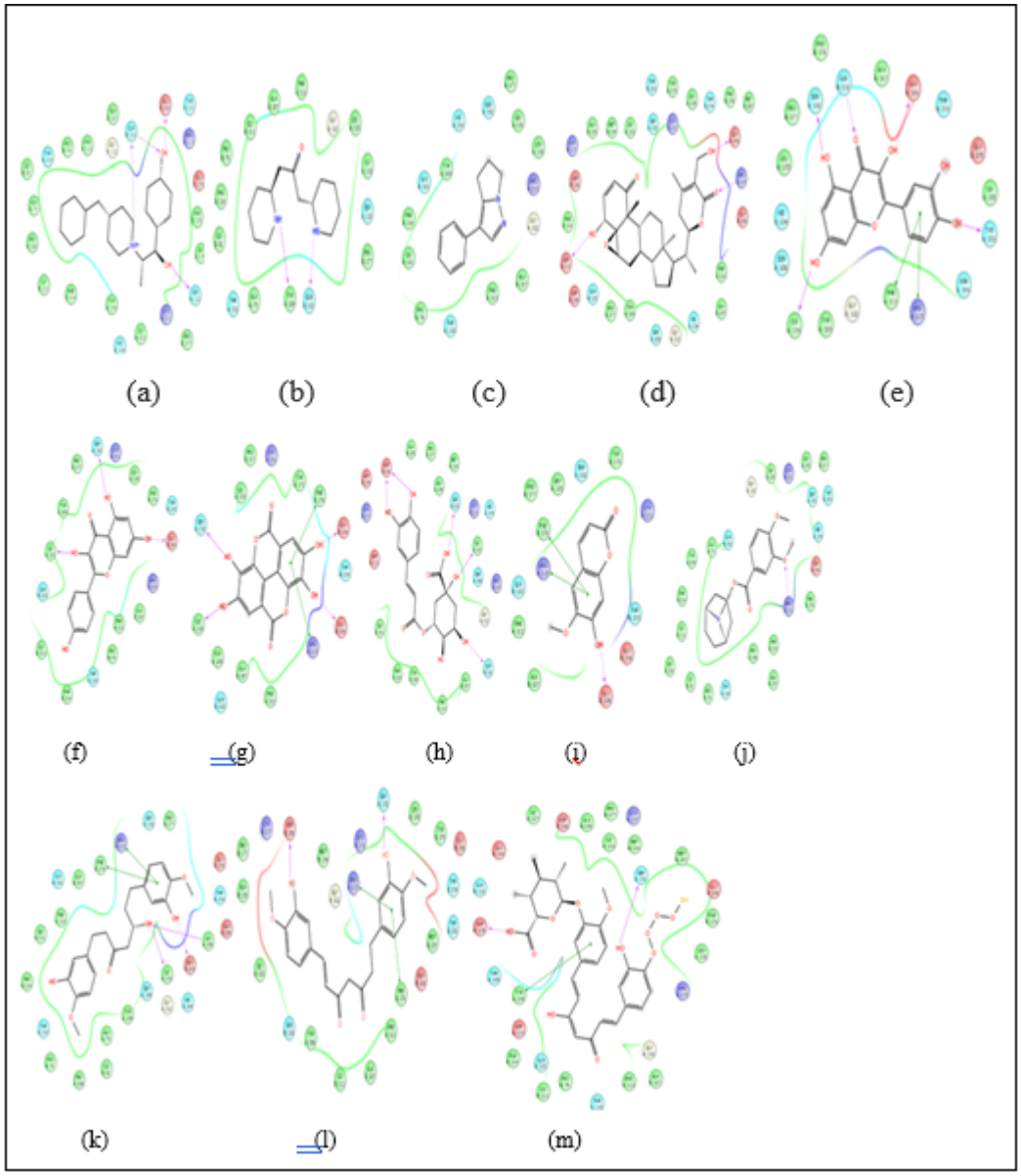

Figure 4: Molecular interaction of top lead phytoconstituents with N-methyl-D-aspartate receptor. (a) QEL 503 (b) Anaferine (c) Withasomnine (d) Withaferin A (e) Quercetin (f) Kaempferol (g) Ellagic Acid (h) Chlorogenic Acid (i) Scopoletin (j) Convolamine (k) Hexahydrocurcumin (l) Dihydrocurcumin (m) Curcumin Glucuronide Sulfate.

are found less toxicity, while Anaferin, Withaferin A, Kaempferol, Convolamine found no toxicity. For toxicity study laxor toxicity predictor software is used Lazar and protox online server was used to predict in silico toxicity (Table 4). For Cytotoxicity and LD_{50}, prediction Protox-II software is used (Table 2).

DISCUSSION

The discussion revolves around the intricate process of ligand docking, from the generation of ligand poses to the evaluation of toxicity and carcinogenicity. Ligand poses, representing the ligand's spatial and conformational relationship with the receptor, are systematically assessed through hierarchical filters, emphasizing the critical role of the initial filter in measuring ligand compatibility with the active site. The use of a grid-based method ensures precise control over ligand-receptor interactions, with a subsequent estimate and minimization of OPLS-AA unbound ligand-receptor interaction energies. The importance of generating a final score for low-energy poses is highlighted, as it serves as a determinant of ligand efficacy. The evaluation of slip results prioritizes visual assessments, leveraging the Glide Exposure Viewer panel of enhanced of enhanced insights in to ligand –receptor interactions. The docking scores table, including Glide Score (G-Score), G-Energy and pose receptor combinations, provides a comprehensive overview of ligand performance in the docking process. Moving beyond docking, the discussion delves in to the validation results, emphasizing the selection of compounds based on functional score predictions for further analysis. The subsequent toxicity study unveils varying toxicity

Table 3: Toxicity Study.

Phytoconstituents	LD_{50}	Hepatotoxicity		Carcinogenicity		Immunotoxicity		Mutagenicity		Cytotoxicity	
		Prediction	Probability	Prediction	Probability	Prediction	Probability	Prediction	Probability	Prediction	Probability
Anaferin	1190mg/kg	Inactive	0.78	Inactive	0.70	Inactive	0.99	Inactive	0.82	Inactive	0..76
Withasomnine	800 mg/kg	Inactive	0.72	Active	0.52	Inactive	0.99	Inactive	0.58	Inactive	0.69
Withaferin A	300 mg/kg	Inactive	0.93	Inactive	0.55	Active	0.99	Inactive	0.79	Active	0.87
Quercetin	159 mg/kg	Inactive	0.69	Active	0.68	Inactive	0.87	Active	0.51	Inactive	0.99
Kaempferol	3919mg/kg	Inactive	0.68	Inactive	0.72	Inactive	0.96	Inactive	0.52	Inactive	0.98
Elagic acid	823 mg/kg	Inactive	0.83	Active	0.59	Inactive	0.81	Inactive	0.84	Inactive	0.90
Chlorogenic acid	5000mg/kg	Inactive	0.72	Inactive	0.68	Active	0.99	Inactive	0.93	Inactive	0..80
Scopoletin	3800mg/kg	Inactive	0.69	Active	0.53	Active	0.54	Inactive	0.56	Inactive	0.91
Convolamine	650 mg/kg	Inactive	0.88	Inactive	0.57	Inactive	0.68	Inactive	0.76	Inactive	0.51
Dihydrocurcuminin	3000mg/kg	Inactive	0.72	Inactive	0.68	Active	0.92	Inactive	0.78	Inactive	0.73
Curcumin glucoronidesulfate	2000mg/kg	Inactive	0.59	Inactive	0.71	Active	0.99	Inactive	0.67	Inactive	0.75

Table 4: Molecular descriptor values of top lead phytoconstituents.

Phytoconstituents	Acute toxicity (Fathead minnow) (mg/L)	Carcinogenicity (Rodents) (multiple species/ sites)	Carcinogenicity (Mouse)	Carcinogenicity (Rat)	Carcinogenicity (Mouse (TD_{50})) (mg/kg_bw/day)	Carcinogenicity (Rat (TD_{50})) (mg/kg_bw/day)	Maximum Recommended Daily Dose (Human) (mg/ kg_bw/day)	Mutagenicity (Salmonella typhimurium)
Withaferin A	32.5	Non-carcinogenic	non-carcinogenic	non-carcinogenic	0.102 (mmol/kg-bw/ day)	0.052(mmol/kg-bw/ day)	28.2	non-mutagenic
Anaferin	41.4	non-carcinogenic	non-carcinogenic	non-carcinogenic	0.118(mmol/kg-bw/ day)	0.062(mmol/kg-bw/ day)	3.27	non-mutagenic
Withasomnine	7.77	non-carcinogenic	non-carcinogenic	carcinogenic	0.12 (mmol/kg-bw/ day) 22.2 (mg/kg_bw/day)	0.0712 (mmol/kg-bw/ day) 13.1 (mg/kg_bw/day)	1.77	Mutagenic
Quercetin	7.69	carcinogenic	non-carcinogenic	carcinogenic	0.167 (mmol/kg-bw/ day) 50.4 (mg/kg_bw/day)	0.0334 (mmol/kg-bw/ day) 10.1 (mg/kg_bw/day)	1.51	Mutagenic
Kaempferol	36.3	non-carcinogenic	non-carcinogenic	non-carcinogenic	8.76 (mmol/kg-bw/ day) 2520.0 (mg/kg_bw/ day)	2.9 (mmol/kg-bw/day) 836.0 (mg/kg_bw/day)	10.5	non-mutagenic
Ellagic acid	28.4	non-carcinogenic	non-carcinogenic	non-carcinogenic	4.59 (mmol/kg-bw/ day) 781.0 (mg/kg_bw/day)	0.823 (mmol/kg-bw/ day) 140.0 (mg/kg_bw/day)	39.4	non-mutagenic
Cholorogenic acid	25.8	Non-carcinogenic	Non-carcinogenic	Non-carcinogenic	3.22(mmol/kg-bw/ day) 601.0 (mg/ kg_bw/day)	0.723(mmol/kg-bw/ day)120.0 (mg/kg_bw/ day)	34.77	non-mutagenic
Scopoletin	15.31	Carcinogenic	non-carcinogenic	non-carcinogenic	0.498 (mmol/kg-bw/ day) 95.7 (mg/kg_bw/day)	0.0887 (mmol/kg-bw/ day) 17.0 (mg/kg_bw/day)	2.67	non-mutagenic
Convolamine	44.1	non-carcinogenic	non-carcinogenic	non-carcinogenic	0.0966 (mmol/kg-bw/ day) 29.5 (mg/kg_bw/day)	0.0041 (mmol/kg-bw/ day) 1.25 (mg/kg_bw/day)	1.05	non-mutagenic
Hexahydrocurcumine	34.2	carcinogenic	carcinogenic	carcinogenic	1.527(mmol/kg-bw/ day) 624.0 (mg/kg_bw/day)	0.643 mmol/kg-bw/ day) 198.0 (mg/kg_bw/day)	5.01	Non-mutagenic
Dihydrocurcumin	30.2	carcinogenic	carcinogenic	carcinogenic	1.42 (mmol/kg-bw/ day) 526.0 (mg/kg_bw/day)	0.518 (mmol/kg-bw/ day) 192.0 (mg/kg_bw/day)	4.84	non-mutagenic
Curcumin glucuronide sulfate	57.3	non-carcinogenic	non-carcinogenic	non-carcinogenic	1.8 (mmol/kg-bw/day) 1090.0 (mg/kg_bw/ day)	0.74 (mmol/kg-bw/day) 447.0 (mg/kg_bw/day)	10.3	non-mutagenic

Carcinogenicity of Quercetin, scopoletin, Hexahydrocurcumine, Dihydrocurcumin found less carcinogenic.

levels among compounds with certain ligands demonstrating lower toxicity and others deemed non-toxic. Carcinogenicity assessments further categorize compounds, identifying potential carcinogens and non-carcinogenic substances. The integrated analysis approach allows for a holistic understanding of ligand behavior, safety implications, and potential therapeutic applications. This discussion sheds light on the multifaceted considerations involved in ligand docking studies, showcasing the complexity and importance of each step in the process.

CONCLUSION

The compounds Anaferin, Withasomnine, Withaferin A, quercetin, kaempferol, ellagic acid, chlorogenic acid, scopolamine, Convolamin, hexahydrocurcumin, dihydrocurcumin, curcumin glucuronic acid sulfate and NMDA receptors have exhibited diverse properties and binding energies. This suggests the potential for utilizing these plant derived substances in the development of novel NMDA receptor antagonists, presenting a promising avenue for the therapeutic intervention in Alzheimer's Disease (AD). However to validate and substantiate the computational findings presented in this study, further investigations through *in vitro* and *in vivo* studies imperative. The comprehensive understanding gained through such experimental endeavors will contribute to the assessment of the therapeutic viability of these compounds in the context of neurodegenerative disorders, particularly Alzheimer's disease.

ACKNOWLEDGEMENT

We authors are thankful to Department of Science and Technology, Government of India, New Delhi for providing funding under SYST project for this research work.

CONFLICT OF INTEREST

The authors declare that there is no conflict of interest.

ABBREVIATIONS

NMDA: N-methyl D-Aspartate; **AD:** Alzheimer's Disease; **ADMET:** Absorption Distribution Metabolism Excretion Toxicity; **GluN2B:** Glutamate receptor subtype 2B; **FDA:** Food Drug Administration; **PDB:** Protein Data Bank; **DCKA:** 5,7 dichloroquinuric acid; **NR1:** Nuclear receptor 1; **PBQ:** Crystal Structure of the NR1 Ligand binding core in complex with 5,7 Dichlorokynurenic acid (DCKA); **RCSB:** Research collaborator for Structural Bioinfrmatics; **OPLS-AA:** Optimized Potentials for Liquid Simulations.

SUMMARY

In summary Ligand poses generated by Glide are passed through a series of hierarchical filters to evaluate ligand-receptor interactions.[22] The first filter measures the compatibility of the ligand with the defined active site and uses a grid-based method to control the addition of ligand-receptor interactions includes estimate to estimate and minimize OPLS-AA unbound ligand-receptor interaction energies.[23] Then made a final score of low-energy poses. Evaluation of slip results focuses on visual rather than numerical evaluation. The glide is displayed from the Glide Exposure Viewer panel.[24] The Table 1 provides docking scores for each pose with combinations of Glide Score (G-Score), G-Energy, and pose receptor.[25] Table 1 shows the results for all compounds and molecular groups used for validation. To analyze the docking results, compounds were selected based on the best matches predicted by the functional scores. Table 4 shows that Withasomnine, quercetin, ellagic acid, chlorogenic acid, scopoletin, Dihydrocurcuminin, Curcumin glucoronide sulfate are found to be less toxic while Anaferin, Withaferin A, Kaempferol, Convolamine found no toxicity. Table 4 shows that Quercetin, scopoletin, Hexahydrocurcumine, Dihydrocurcumin are carcinogenic while other phytochemicals are free from carcinogenicity.

REFERENCES

1. Kvist T, Steffensen TB, Greenwood JR, Mehrzad Tabrizi F, Hansen KB, Gajhede M, *et al.* Crystal structure and pharmacological characterization of a novel N-methyl-D-aspartate (NMDA) receptor antagonist at the GluN1 glycine binding site. J Biol Chem. 2013;288(46):33124-35. doi: 10.1074/jbc.M113.480210, PMID 24072709.
2. Campos-Peña V, Meraz-Ríos MA. Ch 12. Neurochemistry. Mexico City: InTech. Alzheimer disease: the role of A in the glutamatergic system. In: Heinbockel T, editor; 2014.
3. Huang YJ, Lin CH, Lane HY, Tsai GE. NMDA neurotransmission dysfunction in behavioral and psychological symptoms of Alzheimer's disease. Curr Neuropharmacol. 2012;10(3):272-85. doi: 10.2174/157015912803217288, PMID 23450042.
4. Danysz W, Parsons CG. Alzheimer's disease, β-amyloid, glutamate, NMDA receptors and memantine - searching for the connections. Br J Pharmacol. 2012;167(2):324-52. doi: 10.1111/j.1476-5381.2012.02057.x, PMID 22646481.
5. Waqar M, Batool S. *In silico* analysis of binding interaction of conantokins with NMDA receptors for potential therapeutic use in Alzheimer's disease. J Venom Anim Toxins Incl Trop Dis. 2017;23:42. doi: 10.1186/s40409-017-0132-9, PMID 28943883.
6. Kumar A, Nisha CM, SilakariC, SharmaI, AnushaK, GuptaN, *et al.* Current and novel therapeutic molecules and targets in Alzheimer's disease. JFormos Med Assoc. 2016;115(1):3-10. doi: 10.1016/j.jfma.2015.04.001, PMID 26220908.
7. Parsons CG, DanyszW, DekundyA, PulteI. Memantine and cholinesterase inhibitors: complementary mechanisms in the treatment of Alzheimer's disease. Neurotox Res. 2013;24(3):358-69. doi: 10.1007/s12640-013-9398-z, PMID 23657927.
8. Molinuevo JL, Lladó A, Rami L. Memantine: targeting glutamate excitotoxicity in Alzheimer's disease and other dementias. Am J Alzheimers Dis Other Demen. 2005;20(2):77-85. doi: 10.1177/153331750502000206, PMID 15844753.
9. Furukawa H, GouauxE. Mechanisms of activation, inhibition and specificity: crystal structures of the NMDA receptor NR1 ligand-binding core. EMBO J. 2003;22(12):2873-85. doi: 10.1093/emboj/cdg303, PMID 12805203Table 2.
10. Krueger BA, Weil T, Schneider G. Comparative virtual screening and novelty detection for NMDA-glycineB antagonists. J ComputAid Mol Des. 2009;23(12):869-81. doi: 10.1007/s10822-009-9304-1, PMID 19890609.
11. Leong MK, Syu RG, Ding YL, Weng CF. Prediction of N-methyl-D-aspartate receptor GluN1-ligand binding affinity by a novel SVM-pose/SVM-score combinatorial ensemble docking scheme. Sci Rep. 2017;7:40053. doi: 10.1038/srep40053, PMID 28059133.
12. KvistT, GreenwoodJR, HansenKB, TraynelisSF, Bräuner-Osborne H. Structure-based discovery of antagonists for GluN3-containing N-methyl-D-aspartate receptors. Neuropharmacology. 2013;75:324-36. doi: 10.1016/j.neuropharm.2013.08.003, PMID 23973313.
13. Chaieb K, Hajlaoui H, Zmantar T, Kahla-Nakbi AB, Rouabhia M, Mahdouani K, *et al.* The chemical composition and biological activity of clove essential oil, *Eugenia caryophyllata* (*Syzigium aromaticum* L. Myrtaceae): a short review. Phytother Res. 2007;21(6):501-6. doi: 10.1002/ptr.2124, PMID 17380552 (*Syzigium aromaticum* L. Myrtaceae).
14. Nassar MI, Gaara AH, El-Ghorab AH, Farrag A, Shen H, Huq E, *et al.* Chemical constituents of clove. Rev Latinoam Quim. 2007;35:47 (*Syzygium aromaticum*, Fam. Myrtaceae) and their antioxidant activity.

15. Chaudhry AH, Tanveer A, Shar A, Akhtar MS, Shahid MK, Ashfaq KM, *et al.* Physico-chemical investigation and antimicrobial activity of essential oil of *Cuminum cyminum* L. World Appl Sci J. 2012;19:330-3.
16. Khan IU, Mehriya ML, Rathore BS, Kumhar SR, Singh B. Evaluation of volatile phytochemical constituents in cumin (*Cuminum cyminum*) genotypes by gas chromatography-mass spectroscopy. J Pharmacogn Phytochem. 2017;6:768-73.
17. D S, T JZ, N KL, K J. Correlation between chemical profiles of black pepper (*Piper nigrum* L.) var. Panniyur-1 collected from different locations. J Med Plants Res. 2013;7(31):2349-57. doi: 10.5897/JMPR2013.4493.
18. Rao VR, Raju SS, Sarma VU, Sabine F, Babu KH, Babu KS, *et al.* Simultaneous determination of bioactive compounds in *Piper nigrum* L. and a species comparison study using HPLC-PDA. Nat Prod Res. 2011;25(13):1288-94. doi: 10.1080/14786419.2010.535158, PMID 21854175.
19. Jayaprakasha GK, Rao LJ, Sakariah KK. Chemical composition of the volatile oil from the fruits of *Cinnamomum zeylanicum* Blume. Flavour Fragr J. 1997;12(5):331-3. doi: 10.1002/(SICI)1099-1026(199709/10)12: 5<331::AID-FFJ663>3.0.CO;2-X.
20. Kaul PN, Bhattacharya AK, Rajeswara Rao BR, Syamasundar KV, Ramesh S. Volatile constituents of essential oils isolated from different parts of cinnamon (*Cinnamomum zeylanicum* Blume). J Sci Food Agric. 2003;83(1):53-5. doi: 10.1002/jsfa.1277.
21. Okugawa H, Moriyasu M, Matsushita SA, Saiki K, Hashimoto Y, Matsumoto K, *et al.* Evaluation of crude drugs by a combination of enfleurage and chromatography-4-on flavor components in seeds of *Amomum cardamomum* and *Elettaria cardamomum*. Shoyakugaku Zasshi. 1988;42:94-7.
22. Husain SS, Ali M. Analysis of volatile oil of the fruits of *Elettaria cardamomum* (L.) maton and its antimicrobial activity. World J Pharm Pharm Sci. 2014;3:1798-808.
23. Schrödinger Release; Version 3.6. NY: LigPrep, Schrödinger, LLC. 2015;4.
24. Friesner RA, Murphy RB, Repasky MP, Frye LL, Greenwood JR, Halgren TA, *et al.* Extra precision glide: docking and scoring incorporating a model of hydrophobic enclosure for protein-ligand complexes. J Med Chem. 2006;49(21):6177-96. doi: 10.1021/jm051256o, PMID 17034125.
25. Small-moleculedrugdiscoverysuite; Version 4.6. NY: QikProp, Schrödinger, LLC. 2015;4.

Cite this article: Baviskar BA, Deore SL, Shende BA, Khadabadi S, Kide AA. *In silico* and Biological Screening of Phytochemicals against NMDA Receptor for Alzheimer's Disease Therapeutics. Pharmacog Res. 2024;16(2):244-53.